# Electrostriction-enhanced giant piezoelectricity via relaxor-like secondary crystals in extended-chain ferroelectric polymers

Zhiwen Zhu<sup>1,8</sup>, Guanchun Rui<sup>2,8</sup>, Qiong, Li<sup>2</sup>, Elshad Allahyarov<sup>3,4,5</sup>, Ruipeng Li<sup>6</sup>, Thibaut Soulestin<sup>7</sup>, Fabrice Domingues Dos Santos<sup>7</sup>, Hezhi He<sup>1,\*</sup>, Philip L. Taylor<sup>3,\*</sup>, Lei Zhu<sup>2,9,\*</sup>

<sup>1</sup> Laboratory of Polymer Processing Engineering of Ministry of Education, Guangdong Provincial
Key Laboratory of Technique and Equipment for Macromolecular Advance Manufacturing, South
China University of Technology, Guangzhou 510641, P. R. China

<sup>2</sup> Department of Macromolecular Science and Engineering, Case Western Reserve University,

Cleveland, Ohio 44106-7202, United States

<sup>&</sup>lt;sup>3</sup> Department of Physics, Case Western Reserve University, Cleveland, Ohio 44106, United States

<sup>&</sup>lt;sup>4</sup> Institut für Theoretische Physik II: Weiche Materie, Heinrich-Heine-Universität Düsseldorf, D-40225

Düsseldorf, Germany

<sup>&</sup>lt;sup>5</sup> Theoretical Department, Joint Institute for High Temperatures, Russian Academy of Sciences, 13/19

Izhorskaya street, Moscow 125412, Russia

<sup>&</sup>lt;sup>6</sup> National Synchrotron Light Source II, Brookhaven National Laboratory, Upton, New York 11973, United States

<sup>&</sup>lt;sup>7</sup> Piezotech S.A.S., Arkema-CRRA, 69496, Pierre-Benite Cedex, France

<sup>&</sup>lt;sup>8</sup> These authors contributed equally to this work: Zhiwen Zhu, Guanchun Rui

<sup>&</sup>lt;sup>9</sup> Lead contact

<sup>\*</sup>Correspondence: <a href="mailto:lxz121@case.edu">lxz121@case.edu</a> (L. Zhu), <a href="mailto:plt@case.edu">plt@case.edu</a> (P. L. Taylor), <a href="mailto:pmhzhe@scut.edu.cn">pmhzhe@scut.edu.cn</a> (H. He)

**Summary** 

Piezoelectricity in ferroelectric polymers originates from the electrostrictive effect coupled

with a remanent polarization. However, its structural origin remains controversial, and it is not

clear how modifying the electrostriction can further improve piezoelectricity for polymers. Here,

we report that electrostriction can be significantly enhanced in poled poly(vinylidene fluoride-co-

trifluoroethylene) [P(VDF-TrFE)] random copolymers containing extended-chain primary crystals

and relaxor-like secondary crystals in the oriented amorphous fraction (SC<sub>OAF</sub>). As a result of the

high polarizability of dipoles and ferroelectric nanodomains in the SC<sub>OAF</sub>, the inverse piezoelectric

coefficient d<sub>31</sub> reaches as high as 77±5 pm/V for the P(VDF-TrFE) 55/45 copolymer at 55 °C. This

finding not only extends our understanding of piezoelectricity in polymers, but also provides

guidance for further enhancing the piezoelectricity of ferroelectric polymers in the future.

**Keywords:** piezoelectricity, P(VDF-TrFE), oriented amorphous fraction, secondary crystal

2

# Introduction

Electrostriction, a fundamental electromechanical coupling effect, can be observed in all dielectric materials under an electric field.<sup>1,2</sup> For ferroelectrics whose paraelectric phase is centrosymmetric, electrostriction is the origin of piezoelectricity.<sup>3</sup> Namely, piezoelectricity is the electrostriction under the bias of a macroscopic (or permanent) remanent polarization ( $P_{r0}$ ). In the linear dielectric/mechanical regime, the piezoelectric coefficient ( $d_{3j}$ , j = 1, 2, 3) can be expressed as:<sup>1,2</sup>

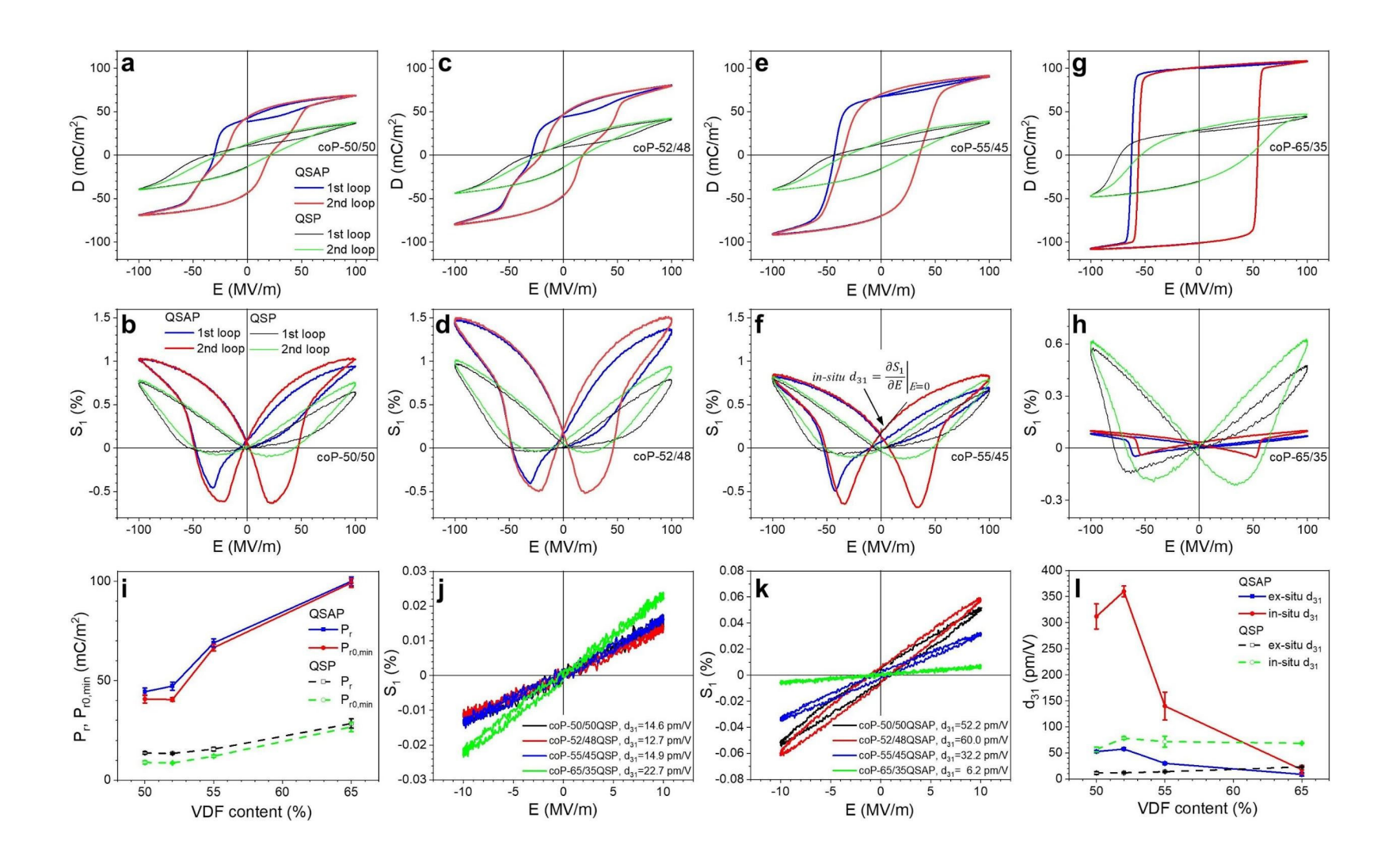
$$d_{3i} = 2\varepsilon_0(\varepsilon_r - 1)Q_{3i}P_{r0}$$
 (Equation 1)

where  $\varepsilon_0$  and  $\varepsilon_r$  are vacuum and relative permittivity and  $Q_{3j}$  the electrostriction coefficient. Therefore, in addition to the bias  $P_{r0}$ , it is possible to utilize electrostriction to enhance piezoelectricity for ferroelectric materials.<sup>2</sup> However, there have been debates about the structural origin for the piezoelectricity in ferroelectric polymers, such as poly(vinylidene fluoride) (PVDF) and its random copolymers, poly(VDF-co-trifluoroethylene) [P(VDF-TrFE)]. That is, which component in the semicrystalline polymers is responsible for their piezoelectricity, the crystalline or the amorphous phase?

The first consideration is the so-called dimensional effect, as mentioned previously.<sup>4,5</sup> Upon the application of mechanical stresses, the volume of the polymer can change, resulting in a change of dipole moment density or polarization. If this is the case, the amorphous phase should provide the major contribution for piezoelectricity, because crystals are less susceptible to volume change under a stress. However, a recent study showed that a morphotropic phase boundary (MPB)-like behavior (often observed for piezoelectric ceramics<sup>6</sup>) was reported for P(VDF-TrFE) with composition around 50/50 (molar ratio), and that the piezoelectricity was enhanced by the helical-to-zigzag conformation transformation in the crystalline domains of P(VDF-TrFE) near the

MPB.<sup>7</sup> However, in-situ dynamic X-ray diffraction measurements on a spin-coated P(VDF-TrFE) 65/35 sample suggested that an additional contribution from the electromechanical coupling between the crystalline lamellae and the amorphous regions should be the primary contribution to piezoelectricity.<sup>4</sup> According to our recent work on highly poled biaxially oriented PVDF with a pure β crystalline phase,<sup>8</sup> this interfacial coupling was realized via the highly mobile, liquid-crystal-like oriented amorphous fraction (OAF) between the crystalline lamella and the isotropic amorphous fraction (IAF).<sup>9</sup> Although our understanding has been advanced by these studies, a question still exists: Does the piezoelectricity comes from the crystalline phase or the OAF? Also, how can we utilize electrostriction to further enhance piezoelectricity?

In this work, a series of P(VDF-TrFE) random copolymers with VDF content from 50 to 65 mol.% was studied (they are denoted as coP-x/y, where x and y are VDF and TrFE molar fractions, respectively; see Figure S1 and Table S1 in the Supplementary Information). Unidirectional poling at 100 MV/m induced highly mobile, relaxor-like secondary crystals in the OAFs (SC<sub>OAF</sub>) of the copolymer films with an extended-chain crystal (ECC) structure. For the quenched (Q), stretched (S), and 130 °C-annealed (A) coP-52/48 film after unipolar poling (P) (coP-52/48QSAP), the in-situ (during the bipolar poling<sup>4,10</sup>) and ex-situ d<sub>31</sub> reached as high as 360±10 and 57.6±2.4 pm/V, respectively. The high piezoelectric performance was attributed to the enhanced electrostriction of the relaxor-like SC<sub>OAF</sub>, rather than that of the extended-chain primary crystals (PCs).



## **Results and discussion**

High piezoelectric performance of P(VDF-TrFE) with an ECC structure. In this study, we mainly focus on the study of d<sub>31</sub>, rather than d<sub>33</sub>, because both the dimensional effect and PC contribution are less significant in the transverse (i.e., stretching) direction than in the longitudinal (i.e., normal) direction. 11 Because non-oriented samples contain piezoelectric contributions from both d<sub>33</sub> (perpendicular to the chains) and d<sub>31</sub> (along the chains), it is necessary to orient the P(VDF-TrFE) samples in order to examine the neat  $d_{31}$  contribution. Surprisingly, the quenched, stretched, and poled (QSP) samples exhibited significantly lower piezoelectric performance than the nonoriented samples. From the literature report. 12 annealing P(VDF-TrFE) in the paraelectric phase above the Curie temperature (T<sub>C</sub>) could lead to an ECC structure. Intriguingly, thermal annealing of the quenched and stretched (QS) samples at 130 °C had a dramatic effect on the piezoelectric performance. Therefore, we start with the effect of semicrystalline structure on the piezoelectric performance by comparing QSP and quenched, stretched, 130 °C-annealed, and poled (QSAP) copolymer films. Figures 1a-h present the first two continuous electric displacement-electric field (D-E) and transverse strain-electric field (S<sub>1</sub>-E) loops at 100 MV/m for QSP and QSAP films with different VDF contents. Prior to the bipolar poling, these samples were unidirectionally poled at 100 MV/m for 60 cycles to achieve a permanent remanent polarization (P<sub>r0</sub>). In-situ (P<sub>r</sub>) and the minimum P<sub>r0</sub> (P<sub>r0,min</sub>) were obtained from these D-E loops; see Supplementary Note 2 and Figure S2 for details. Note that P<sub>r0,min</sub> was slightly lower than the in-situ P<sub>r</sub>, because certain poled ferroelectric domains relax over time after electric poling.<sup>13</sup> From Figure 1i, the P<sub>r</sub> and P<sub>r0,min</sub> values were much higher for the QSAP samples than for the QSP samples. This is ascribed to the much smaller domain sizes in the OSP films than in the OSAP films (note, thermal annealing above T<sub>C</sub> not only produced ECCs, but also grew large ferroelectric domains). <sup>12</sup> Due to the much higher  $P_{r0}$  of the QSAP samples, higher piezoelectric performance is expected.

The ex-situ  $d_{31}$  was measured using bipolar D-E loops at a low field for QSP (Figure 1j) and QSAP films (Figure 1k). In addition to the ex-situ d<sub>31</sub>, the in-situ d<sub>31</sub> can also be obtained from the slopes of the S<sub>1</sub>-E loops at E = 0 during high-field bipolar poling:  $d_{31} = (\partial S_1/\partial E)|_{E=0}$  (Figure 1b.d.f.h).<sup>4,10</sup> The ex-situ d<sub>31</sub> values for different OSP films were around 15-25 pm/V, which are typical for P(VDF-TrFE) copolymers reported in literature. <sup>14</sup> However, the ex-situ d<sub>31</sub> values for the QSAP samples were significantly higher when the VDF content was below 55 mol.% (Figure 11). For example, the highest ex-situ  $d_{31}$  of 57.6 $\pm$ 2.4 pm/V was obtained for coP-52/48QSAP, much higher than that (12.0±0.9 pm/V) of coP-52/48QSP. It seems that the drastically different ex-situ d<sub>31</sub> values for the coP-52/48 QSAP and QSP films could not be simply explained by the MPB-like behavior reported for P(VDF-TrFE) around the 50/50 composition.<sup>7</sup> When the VDF content was increased to 65 mol.%, the ex-situ d<sub>31</sub> significantly decreased to 9.0±3.3 pm/V for coP-65/35QSAP, even lower than that (23.2±0.6 pm/V) of coP-65/35QSP. Intriguingly, the in-situ d<sub>31</sub> values were much higher than the ex-situ d<sub>31</sub> values, especially when the VDF content was below 55 mol.% (Figure 11). For example, the in-situ d<sub>31</sub> for coP-52/48QSAP was 360±10 pm/V, a factor of 5 times larger than that of the ex-situ  $d_{31}$ . The reason for the higher in-situ  $d_{31}$  will be discussed later. However, the ex-situ  $d_{31}$  is more important than the in-situ  $d_{31}$  for practical piezoelectric applications.

In addition to d<sub>31</sub>, d<sub>33</sub> values were also determined using the direct piezoelectric measurement, as reported before.<sup>8</sup> Figure S3 shows the direct charge measurement results, and large d<sub>33</sub> values were obtained for all QSAP films at room temperature. For example, the maximum -d<sub>33</sub> value of coP-52/48QSAP was 69±1.3 pC/N. As shown in Table 1, both d<sub>31</sub> and d<sub>33</sub> values of the low VDF content QSAP films are higher than those reported in literature.<sup>3,7,8,15-21</sup>

**Table 1.** Reported d<sub>31</sub> and d<sub>33</sub> values for different PVDF and P(VDF-TrFE) random copolymers.

Sample <sup>a</sup>	$d_{33}\ ^{b}$	Ref.	Sample <sup>a</sup>	$d_{31}\ ^b$	Ref.
BO PVDF	-62	8	BO PVDF	22	8
UO PVDF	-26	3	UO PVDF	21	17
UO PVDF	-34	15	UO PVDF	22	18
UD P(VDF-TrFE) 81/19	-18	16	UO PVDF	30	19
UO P(VDF-TrFE) 78/22	-39	3	UD P(VDF-TrFE) 73/27	8	20
UO P(VDF-TrFE) 65/35	-35	3	UD P(VDF-TrFE) 65/35	9	20
UD P(VDF-TrFE) 52/48	-44	3	UD P(VDF-TrFE) 52/48	15	20
UD P(VDF-TrFE) 50/50	-63.5	7	UO P(VDF-TrFE) 52/48	43	21
UO P(VDF-TrFE) 50/50 QSAP	-63	this work	UO P(VDF-TrFE) 50/50 QSAP	53	this work
UO P(VDF-TrFE) 52/48 QSAP	-69	this work	UO P(VDF-TrFE) 52/48 QSAP	58	this work
UO P(VDF-TrFE) 55/45	-52	this	UO P(VDF-TrFE) 55/45	30 (22°C)	this
QSAP		work	QSAP	77 (55°C)	work
UO P(VDF-TrFE) 65/35	-37	this	UO P(VDF-TrFE) 65/35	9	this
QSAP		work	QSAP		work

a BO, UO, and UD stand for biaxially oriented, uniaxially oriented, and undrawn, respectively. b The unit of  $d_{33}$  and  $d_{31}$  is pC/N or pm/V.

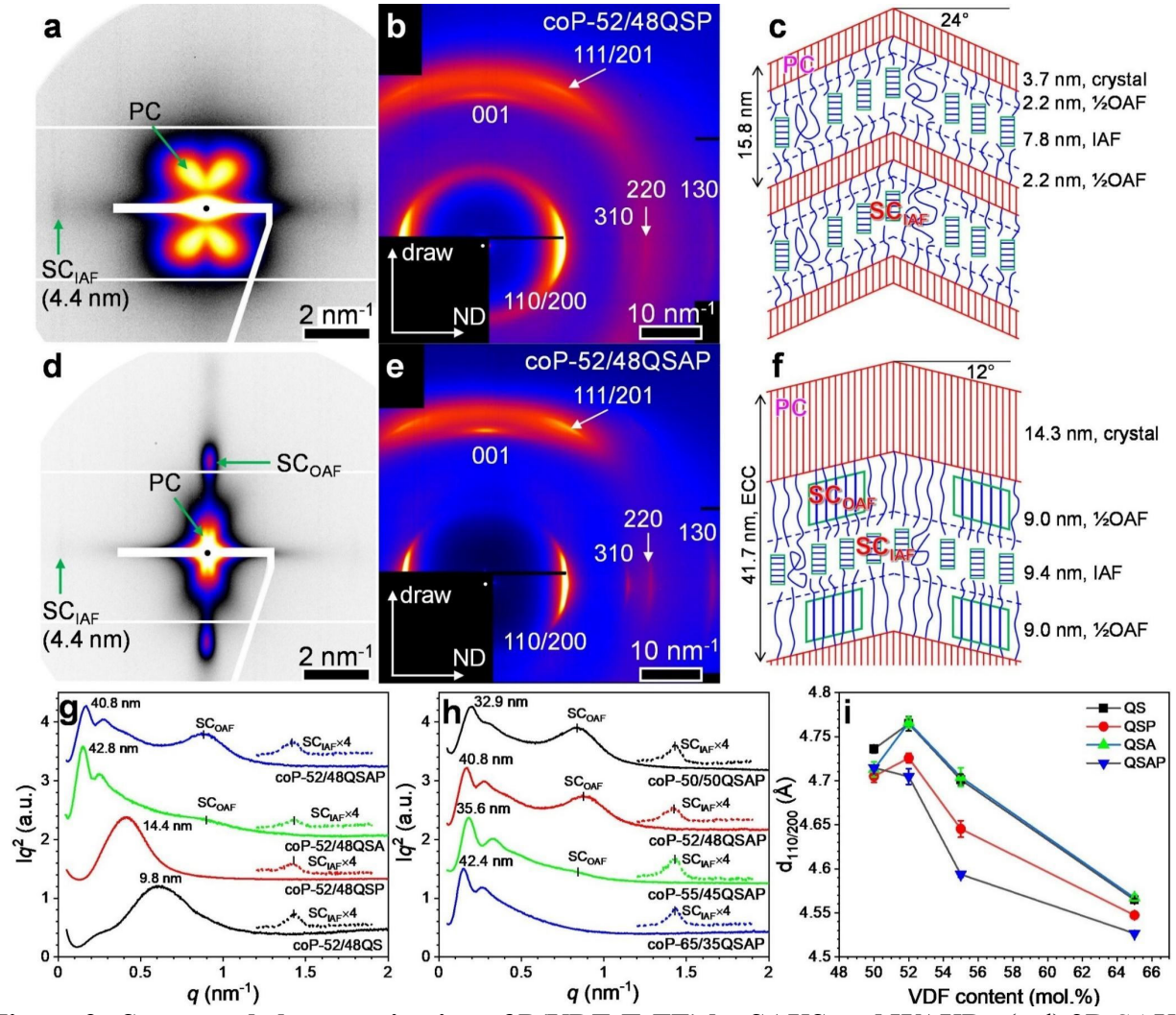


**Figure 2. Structural characterization of P(VDF-TrFE) by SAXS and WAXD.** (a,d) 2D SAXS and (b,e) 2D WAXD patterns of (a,b) coP-52/48 QSP and (d,e) coP-52/48 QSAP films. Proposed semicrystalline structures for (c) coP-52/48QSP and (f) coP-52/48QSAP films. (g) 1D SAXS profiles of the coP-52/48 QS, QSP, QSA, and QSAP films (integrated along the meridian). (h) 1D SAXS curves of coP-50/50QSAP, coP-52/48QSAP, coP-55/45QSAP, and cop-65/35QSAP films. The dotted curves in (g) and (h) are obtained by integration along the equator of the 2D SAXS patterns. (i) The *d*-spacing of the (110/200) reflection for different P(VDF-TrFE) samples at room temperature.

Electric poling-induced SCoAF in the ECC structure. To understand the high ex-situ d<sub>31</sub> for the QSAP copolymers with a low VDF content, synchrotron small-angle X-ray scattering (SAXS) and wide-angle X-ray diffraction (WAXD) experiments were carried out. The results are shown in Figure 2 and Figures S4 and S5. Figure 2a shows the two-dimensional (2D) SAXS pattern of coP-52/48QSP. A butterfly pattern was observed, indicating tilted PCs at ~66° from the stretching

direction (Figure 2c). From 1D correlation function analysis (SasView, v.5.0.2), the PC lamellar spacing (L) was calculated to be L = 14.4 nm (Figure S6b). In addition to the PC lamellar scattering, a weak scattering was seen on the equator (~4.4 nm), and it could be attributed to the stacking of secondary crystals in the IAF (SC<sub>IAF</sub>, see Figure 2c).

The 2D SAXS pattern of coP-52/48QSAP is presented in Figure 2d. Again, a butterfly pattern was seen near the beam center, indicating much thicker tilted PC lamellae (~78° from the stretching direction, see Figure 2f). The lamellar spacing was L = 40.8 nm (Figure S6d), indicative of ECCs in coP-52/48QSAP. Meanwhile, a weak SC<sub>IAF</sub> scattering (~4.4 nm) was observed on the equator. Besides PC and SC<sub>IAF</sub> scatterings, a tear drop-like scattering was observed on the meridian (Figure 2d), this corresponded to the broad scattering peak at 0.88 nm<sup>-1</sup> (6.7 nm) in the corresponding 1D SAXS curve (Figure 2g). The in-situ heating SAXS/WAXD results (Figure S7) showed that this tear drop-like scattering disappeared at ~55 °C; we conclude that it must originate from the SC<sub>OAF</sub>. Figure S8 shows the fast Fourier transform simulation of the SAXS pattern from a sandwiched SC<sub>OAF</sub>/SC<sub>IAF</sub>/SC<sub>OAF</sub> structure. These patterns fit well with the SC<sub>OAF</sub> and SC<sub>IAF</sub> scatterings in Figure 2d. For coP-52/48QSA, the SC<sub>OAF</sub> scattering was less obvious (Figure S4c), showing that unipolar electric poling at 100 MV/m induced the growth of SC<sub>OAF</sub> in the ECC structure. Meanwhile, no SC<sub>OAF</sub> scattering was be observed for coP-52/48QS (Figure S4a) and coP-52/48QSP (Figure 2a), possibly due to the nanoconfinement in thin OAF layers (see Figure 2c). The SC<sub>OAF</sub> scattering was also observed for coP-50/50QSAP. It was fairly weak for coP-55/45QSAP and disappeared for coP-65/35QSAP (Figure 2h and Figures S5a,c,e). As shown in Figure 11, the ex-situ d<sub>31</sub> decreased with increasing the VDF content and became very low (only 9.0 pm/V) for coP-65/35QSAP. These results confirm that electric poling-induced SC<sub>OAF</sub> in the ECC structure was responsible for the high piezoelectric performance of coP-50/50QSAP and coP-52/48QSAP at room temperature.

However, there is still a question: Why couldn't the SC<sub>OAF</sub> be obtained for coP-65/35QSAP, even though it had an ECC structure (L = 42.4 nm, see Figure 2h)? This question was answered by using quantitative 2D WAXD analysis. The 2D WAXD patterns of coP-52/48QSP and coP-52/48QSAP are shown in Figures 2b and 2e, respectively. In these patterns, PCs gave well-defined sharp reflections as indexed. The oriented, halo-like scatterings around the sharp PC reflections should originate from both OAF and SCs.<sup>22</sup> At this moment, it is difficult to differentiate the liquid crystal-like OAF from SCs in WAXD, because SCs also had a poorly ordered structure. In areas free of crystal reflections and OAF scattering, the IAF scattering was identified. Based on our previous report,<sup>22</sup> the contents of PCs ( $x_c$ ), OAF/SC ( $x_{OAF/SC}$ ), and IAF ( $x_{IAF}$ ) could be determined from the 2D WAXD patterns (see Figure S9 and Table S2). The  $x_c$ ,  $x_{OAF/SC}$ , and  $x_{IAF}$  of 52/48QSP were calculated to be 0.25, 0.28, and 0.47, respectively (Figure S9f). For coP-52/48QSAP,  $x_c$ ,  $x_{\text{OAF/SC}}$ , and  $x_{\text{IAF}}$  were 0.36, 0.43, and 0.21, respectively (Figure S9d). Combining both SAXS and WAXD analyses with an assumption that the densities of PC, OAF, and IAF being 1.916, 1.843, and 1.770 g/cm<sup>3</sup> (see Table S3), the semicrystalline structures of coP-52/48QSP and coP-52/48QSAP are shown in Figures 2c and 2f, respectively. For coP-52/48QSP, the OAF layer thickness was too thin ( $t_{OAF} = 2.2 \text{ nm}$ ) to grow SC<sub>OAF</sub>. However, the OAF layer was thick ( $t_{OAF} =$ 9.0 nm) enough to grow SC<sub>OAF</sub> in coP-52/48SQAP. The ECC structure was thus shown to be important for SC<sub>OAF</sub>. As the VDF content increased,  $x_c$  gradually increased,  $x_{OAF/SC}$  decreased, and  $x_{\rm IAF}$  remained mostly unchanged at around 0.21 (Figures S9d,i,j,k). The high  $x_{\rm c}$  (0.55) and the low  $x_{\text{OAF/SC}}$  (0.22,  $t_{\text{OAF}} = 4.8 \text{ nm}$ ) of coP-65/35QSAP prevented the growth of SC<sub>OAF</sub> in the ECC structure.

In addition to  $x_{OAF/SC}$ , another important factor for electrostriction and piezoelectricity is the dipole mobility or  $\varepsilon_r$  in OAF and SC<sub>OAF</sub>, which can be evaluated from the linear dielectric constant using broadband dielectric spectroscopy (BDS, see Figures S10-13). For coP-

65/35QSAP, a low  $\varepsilon_r$  of 10.8 was observed at room temperature and 1 kHz (Figure S13g), significantly lower than that (21.5) of coP-52/48QSAP (Figure S13c). Because the OAF is directly tethered to PCs, the chain-packing in PCs must affect its mobility. Figure 2i presents the interchain spacing of the (110/200) planes (d<sub>110/200</sub>) for different copolymers. First, coP-50/50 and coP-52/48 had a high  $d_{110/200}$  of 4.70-4.77 Å, and coP-65/35 had the lowest  $d_{110/200}$  around 4.54-4.58 Å. Second, after electric poling at 100 MV/m, d<sub>110/200</sub> decreased due to electric field-induced dipoledipole interactions in the PCs. The decrease was small for coP-50/50 and coP-52/48 because of their defective crystal structures; however, it was significant for coP-55/45 and coP-65/35. Because coP-65/35QSAP had the tightest chain-packing, it was expected that the mobility of its OAF should be the lowest, and a low piezoelectric performance was indeed obtained. On the other hand, the piezoelectric performance of coP-52/48QSAP was high due to both high x<sub>OAF/SC</sub> and dipole mobility in the OAF/SC<sub>OAF</sub>. The contents of SC<sub>OAF</sub> and SC<sub>IAF</sub> were estimated by temperaturemodulated differential scanning calorimetry (TMDSC), as shown in Figure S14. For coP-52/48QSAP, the SC<sub>OAF</sub> and SC<sub>IAF</sub> contents were about 5.9% and 3.8%, respectively. With such a low content, it is not possible for us to determine the chain conformation and structure of the SC<sub>OAF</sub>. However, SC<sub>OAF</sub> should be a mesophase, which has a poor crystalline order, rather than the liquid crystalline structure in the OAF.

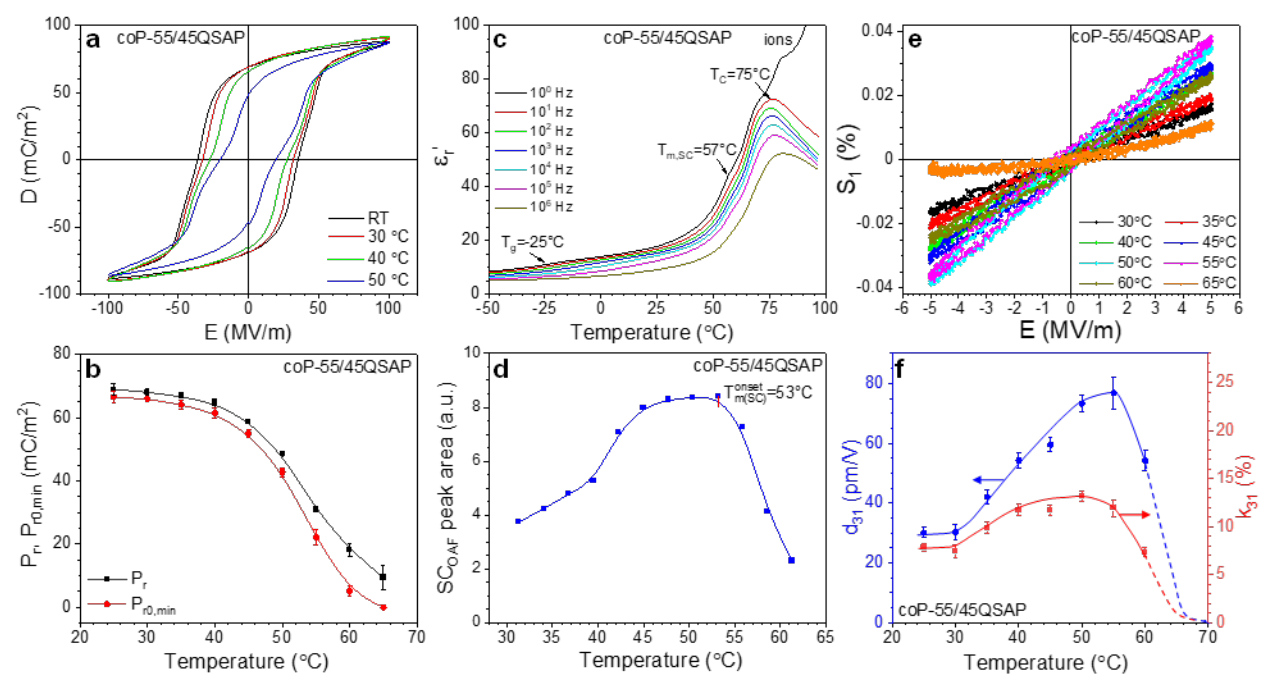


Figure 3. Temperature dependent piezoelectric property in coP-55/45QSAP. (a) Bipolar D-E loops at different temperatures. (b) Temperature dependent  $P_r$  and  $P_{r0,min}$ . (c) Temperature-scan  $\epsilon_r$ ' spectra. (d) Peak area of  $SC_{OAF}$  in 1D SAXS curves (Figure S16c) as a function of temperature. (e) Bipolar  $S_1$ -E loop at different temperatures. The poling field is 5 MV/m at 1 Hz. (f) Temperature-dependent  $d_{31}$  and  $k_{31}$ .

Thermally activated relaxor-like SC<sub>OAF</sub> to further enhance piezoelectricity. According to Equation (1), both  $P_{r0}$  and  $\varepsilon_r$  (i.e., dipole mobility) are important for polymer piezoelectricity. However, which factor is more important? To answer this question, temperature-dependent experiments were carried out. First, bipolar D-E loops were used to study freshly poled coP-55/45QSAP at different temperatures. In-situ  $P_r$  values were obtained from the centered second bipolar loops in Figure 3a, and the  $P_{r0,min}$  values were obtained from Figure S15. Below 40 °C,  $P_{r0,min}$  decreased slightly with increasing temperature. However, it decreased faster above 40 °C. Finally,  $P_{r0,min}$  became zero at 65 °C. Figure 3c shows temperature-scan  $\varepsilon_r$ ' BDS result for coP-55/45QSAP. In addition to a glass transition temperature ( $T_g$ ) around -20 °C and a  $T_C$  around 75 °C, a shoulder peak was seen around 57 °C at 1 Hz. During the in-situ heating SAXS/WAXD experiments (Figure S16), the intensity of the SC<sub>OAF</sub> scattering in SAXS first increased above

40 °C, and then decreased above 53 °C (Figure 3d), suggesting the onset of SC<sub>OAF</sub> melting. Therefore, the shoulder peak at 57 °C in the  $\varepsilon_{r}'$  plot (Figure 3c) could be attributed to the relaxor-like behavior of SC<sub>OAF</sub>. For example, at 55 °C the  $\varepsilon_{r}'$  of coP-55/45QSAP was as high as 44 at 1 Hz, indicative of an enhanced dipole mobility for better piezoelectricity.

Figure 3e shows temperature-dependent  $S_1$ -E loops for coP-55/45QSAP, from which the ex-situ  $d_{31}$  values were obtained (Figure 3f). The  $d_{31}$  increased with increasing temperature. At 55 °C, it reached an unprecedentedly high value of 77±5 pm/V, more than twice that (32.2 pm/V) at room temperature. The coupling factor  $k_{31}$  was calculated from the Young's modulus (Y<sub>1</sub>) (Figure S17) and dielectric constant ( $\varepsilon_{r'}$  at 1 Hz in Figure 3c), <sup>1,8</sup> and had a maximum value of 0.13 at 50 °C. Note that the  $P_{r0,min}$  at 55 °C was only 22.1±2.3 mC/m<sup>2</sup>, nearly 1/3 of that at room temperature. Combining the results in Figures 3b and 3f, we conclude that the mobility of dipoles in relaxor-like SC<sub>OAF</sub> was more important than  $P_{r0}$  for piezoelectricity. Above 55 °C, the SC<sub>OAF</sub> melted and  $P_{r0,min}$  continued to decrease. As a result, the piezoelectric performance sharply dropped at 60 °C. Finally, at 65 °C a combination of piezoelectricity ( $S_1 \propto E$ ) and electrostriction ( $S_1 \propto E^2$ ) could be observed in Figure 3e.

Similar temperature-dependent studies were also performed for coP-52/48QSAP. Upon heating, both  $P_r$  and  $P_{r0,min}$  monotonically decreased (Figures S18a,b). In the BDS spectra in Figure S18c, an obvious shoulder peak was observed around 38 °C ( $\varepsilon_r' = 39$  at 1 Hz), which was attributed to the SC<sub>OAF</sub> melting as evidenced by the temperature dependent SAXS result in Figure S18d. From the S<sub>1</sub>-E loops in Figure S18e, the ex-situ d<sub>31</sub> kept nearly constant ( $\sim$ 56 pm/V) below 35 °C, above which it quickly decreased due to the melting of the relaxor-like SC<sub>OAF</sub> and decreased  $P_{r0}$  (Figure S18f).

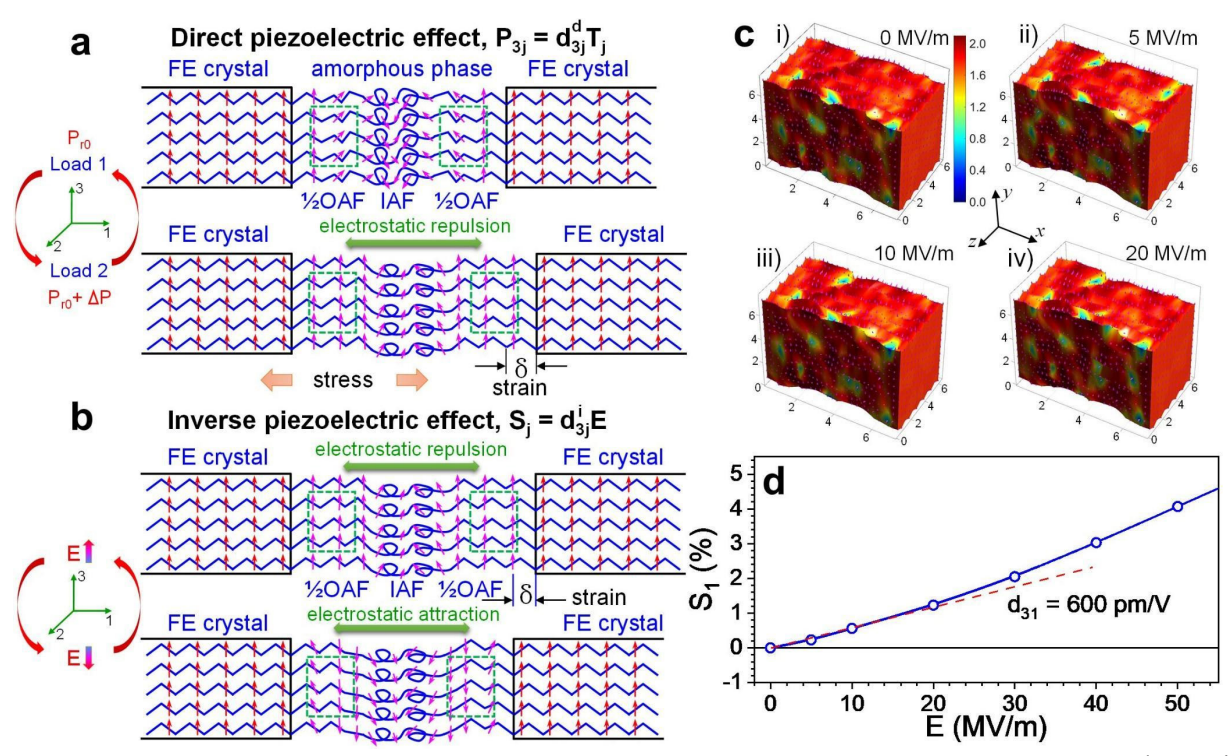


**Figure 4.** Computer simulation of inverse piezoelectricity in PVDF polymers. Schematic illustrations of (a) direct and (b) inverse piezoelectric effects. The green dashed boxes represent  $SC_{OAF}$ , and  $SC_{IAF}$  is not drawn for simplicity. For ferroelectric piezoelectrics with a  $C_{2v}$  symmetry, the longitudinal direction is 3 and the transverse direction is 1. (c) Simulation slabs for PVDF under (i) 0, (ii) 5, (iii) 10, and (iv) 20 MV/m at 300 K. The color scale represents PVDF units with positive dipole moments along y with values between 0 (blue) and 2.1 D (red). Chain ends are attached to both slab walls with a rigid C-C bond (i.e., dipole moment fixed along the y-axis). The attachment points are organized in the same manner as the β PVDF crystal. (d) Simulated  $S_1$  as a function of applied electric field for the PVDF chains between the slab walls.

Mechanism of electrostriction-enhanced piezoelectricity via relaxor-like  $SC_{OAF}$  and the theoretical limit. From the above studies, high dipole mobility in the relaxor-like  $SC_{OAF}$  is considered to be the key to the high piezoelectricity of some P(VDF-TrFE) with an ECC structure. This can be further elaborated using the schematics in Figures 4a and 4b for direct and inverse piezoelectricity, respectively. From our recent report,<sup>8</sup> we understand that electrostriction in ferroelectric polymers has two origins: mechano-electrostriction due to the conformation transformation and electrostatic interaction between ferroelectric nanodomains. The electrostriction coefficient is closely related to  $\varepsilon_r$  and the mechanical modulus  $(Y_j)$  of the sample via an empirical relationship:  $Q_{3j} \propto (\varepsilon_r Y_j)^{-1} \cdot ^{22,23}$  For the direct piezoelectricity (Figure 4a), a

transverse stress ( $T_1$ ) induces an instantaneous strain,  $S_1$ , which leads to a conformation transformation of the OAF to increase the polarization ( $P+\Delta P$ ).<sup>8</sup> In this sense, mechanoelectrostriction is more important for the direct piezoelectric effect. For the inverse piezoelectricity (Figure 4b), an external electric field (which is far below the coercive field at 30-50 MV/m) can polarize the mobile dipoles in the OAF either up or down, while the  $P_{r0}$  in the ferroelectric PCs is fixed in the up direction. When the OAF dipoles are up, an electrostatic repulsion is induced between parallel-aligned ferroelectric crystals and the OAFs; therefore, the sample expands in the transverse direction. When the OAF dipoles are down, an electrostatic attraction is induced between anti-parallel ferroelectric crystals and the OAFs; therefore, the sample shrinks in the transverse direction. We can see that both mechano-electrostriction and electrostatic interactions are important for inverse piezoelectricity.

When relaxor-like  $SC_{OAF}$  exists in the OAF, the polar nanoregions or nanodomains can further enhance electrostriction via an increased  $\varepsilon_r$ . Due to the extremely poor crystal structure of  $SC_{OAF}$ , the modulus may not increase much for the entire OAF layer. As a result, the overall piezoelectric performance is further improved by the relaxor-like  $SC_{OAF}$ . Because the  $SC_{OAF}$  melts at a temperature close to  $T_C$ , it is impossible for us to obtain a piezoelectric QSAP sample without any  $SC_{OAF}$  and compare the piezoelectric performance. However, we could compare the  $Q_{31}$  values between the QSAP and QSA samples. If the  $Q_{31}$  of the QSAP sample is higher than that of the QSA sample, we can prove that the relaxor-like  $SC_{OAF}$  enhances piezoelectricity via electrostriction. First, the  $Q_{31}$  of coP-52/48QSA was determined using the low-field (<30 MV/m) electrostriction method, as we reported before (see Figure S20):<sup>22</sup>  $Q_{31} = 2.47 \pm 0.03$  m<sup>4</sup>/C<sup>2</sup>. Second, the  $Q_{31}$  of coP-52/48QSAP could not be measured using the electrostriction method, because it was piezoelectric. Instead, it was calculated using Equation (1) with  $d_{31} = 57.6 \pm 2.4$  pm/V,  $P_{r0} = 40.5 \pm 0.9$  mC/m<sup>2</sup>, and  $\varepsilon_r = 26.4$  at 1 Hz:  $Q_{31} = 3.20 \pm 0.15$  m<sup>4</sup>/C<sup>2</sup>. The higher  $Q_{31}$  for coP-52/48QSAP

than coP-52/48QSA, therefore, clearly confirmed that electrostriction from SC<sub>OAF</sub> increased piezoelectricity for coP-52/48QSAP.

In addition, the electrostriction from nanodomains in the OAF/SC<sub>OAF</sub> was further enhanced during the high-field bipolar poling. For example, as shown in Figure 11, the in-situ d<sub>31</sub> during 100 MV/m poling is much higher than the ex-situ d<sub>31</sub> for both QSP and QSAP samples, especially for the low-VDF-content copolymers. As reported recently,<sup>24</sup> ferroelectric domains can be induced in the OAF when the poling field is above 25 MV/m. It is the enhanced electrostriction via relaxor nanodomains in the OAF/SC<sub>OAF</sub> that leads to the high in-situ d<sub>31</sub> of P(VDF-TrFE) copolymers.

The giant in-situ  $d_{31}$  of 360 pm/V for coP-52/48QSAP drives us to ask the question: what is the theoretical limit of  $d_{31}$  for PVDF-based polymers? To obtain the answer to this question, we turn to a full-atomistic molecular dynamics (MD) simulation, in which the inverse piezoelectric effect is simulated for PVDF with fully oriented  $\beta$  crystals (for details see MD simulation in Supplementary Note 17).<sup>8</sup> In brief, we built a 12×12 array of PVDF chains tethered to two (crystal) walls, where the *ab*-unit cell dimensions are a = 1.05 nm and b = 0.6 nm (a slightly larger *ab*-unit cell than that of the  $\beta$  phase was used to speed up the simulation). For the tethered repeat units, the dipole moments were fixed in the y direction. Upon the application of an electric field along the y axis, the PVDF dipoles rotated, causing the chains to extend in the x direction; see Figure 4c. The transverse strain, S<sub>1</sub>, is plotted as a function of the applied field in Figure 4d. As we can see, when the electric field was below 20 MV/m, a linear relationship was observed, which is the inverse piezoelectric effect. From the slope, the inverse  $d_{31}$  was estimated to be 600 pm/V. This theoretical limit confirms that the validity of the ultrahigh in-situ  $d_{31}$  value (360 pm/V) for coP-52/48QSAP.

## 3. Conclusion

In summary, high piezoelectric performance (ex-situ  $d_{31} = 58-77$  pm/V) was achieved for low-VDF-content P(VDF-TrFE) QSAP films with an ECC structure. Structural analyses indicated the existence of electric poling-induced SC<sub>OAF</sub> with an estimated content of ~5.9%. Upon heating, dipoles and possible nanodomains in the SC<sub>OAF</sub> became highly mobile, leading to a relaxor-like behavior. Given the ultrahigh  $d_{31}$  values, i.e., 600 pm/V predicted by simulation and 360 pm/V insitu  $d_{31}$  for coP-52/48QSAP, we are confident that even higher piezoelectric performance is attainable, if the SC<sub>OAF</sub> content can be further increased.

## **EXPERIMENTAL PROCEDURES**

# **Resource Availability**

Lead Contact

Further information and requests for resources and reagents should be directed to and will be fulfilled by the Lead Contact, Lei Zhu (lxz121@case.edu).

# Materials Availability

This study did not generate new reagents. Vinylidene fluoride (VDF) and trifluoroethylene (TrFE) monomers were supplied by Arkema, Inc., Lyon, France. Suspension copolymerization was carried at Piezotech, Inc., a subsidiary of Arkema, Inc.

## Data and Code Availability

The authors declare that all data supporting the findings of this study are available within the paper and its Supplementary Information file or from the lead contact upon reasonable request.

# Synthesis of P(VDF-co-TrFE) Random Copolymers by Suspension Polymerization

VDF and TrFE comonomers were transferred into a 3-L autoclave reactor containing deionized water and a hydroxypropylmethyl cellulose stabilizer at room temperature, following a similar suspension polymerization process reported before.<sup>25</sup> The reactor was heated up to 44 °C. The pressure drop inside the autoclave was compensated by the injection of deionized water. After the introduction of 700 g of deionized water, the injection stopped, and the pressure dropped. When the pressure was stable, the autoclave was cooled down to 17 °C. After degassing, the crude product (a white powder) was filtered. The resulting fine white powder was washed with deionized water. The final product was dried for 24 h at 60 °C in a ventilated oven (yield > 90%).

## **Molecular Characterization**

The proton nuclear magnetic resonance (<sup>1</sup>H NMR) spectra were recorded on a Bruker Ascend III 500 MHz with a prodigy probe. Deuterated acetonitrile was used as the solvent. The water peak was shifted to lower fields (>8 ppm) by adding a small amount of trifluoroacetic acid. The copolymer molar composition is determined using the following equation:

$$\%mol\ TrFE = \frac{n_{VDF}}{n_{VDF} + n_{TrFE}} \times 100\%$$
 (Equation 2)

where  $n_{VDF}$  and  $n_{TrFE}$  are moles of VDF and TrFE repeat units in the copolymers, respectively:  $n_{TrFE} = \int_{4.9}^{5.9} CHFdH$  and  $n_{VDF} = \frac{1}{2} \int_{2.2}^{3.4} CH_2 dH$ . The <sup>1</sup>H NMR spectra of the P(VDF-TrFE) random copolymers are shown in Figure. S1.

The weight-average molecular weights  $(M_w)$  were determined by size-exclusion chromatography (SEC) using a Waters P600 pump, two columns PSS PFG 1000A and PSS PFG 1000A, and a Waters 2414 differential refractive index detector. Dimethyl sulfoxide (DMSO) was used as the solvent, and the flow rate was 1.0 mL/min. PMMA standards were used for

conventional calibration. The powder was dissolved at 95 °C during 4 h in DMSO at a 2 g/L concentration. Melt flow index (MFI) was tested by a LMI5000 melt flow indexer from Dynisco (Oxford, GA) with 10 kg weight at 230 °C. The molecular characterization data are summarized in Table S1.

## Film Fabrication and Processing

Four types of film samples were fabricated via different combinations of hot-pressing, quenching (Q), stretching (S), annealing (A), and poling (P). i) Ouenched and stretched (OS) samples. Using nonsticking aluminum foils, P(VDF-TrFE) random copolymers were hot-pressed at 200 °C, followed by quenching into liquid nitrogen. The quenched films (~50 µm) were uniaxially stretched to an extension ratio of ca. 500% using a home-built stretching apparatus at room temperature. ii) Quenched, stretched, and poled (QSP) samples. The QS films were unidirectionally polarized under 100 MV/m (i.e., 50 MV/m DC + 50 MV/m AC at 1 Hz) for 60 cycles at room temperature. iii) Quenched, stretched, and annealed (OSA) samples. The QS films were annealed at 130 °C for 48 h (coP-50/50 and coP-52/48), 24 h (coP-55/45), and 12 h (coP-65/35), respectively, using an Instec HCS402 hot-stage (Instec, Inc., Boulder, CO). Different lengths of the annealing time were determined by two considerations. First, the annealing time should be long enough to achieve the ECC structures. Second, it was observed that prolonged annealing at 130 °C caused the brittleness of the QSA films, which prevented later piezoelectric study, especially for the high VDF content copolymers. This is attributed to the increased crystallinity and possibly disentanglement of polymer chains due to the sliding motion in the paraelectric samples. 12 iv) Quenched, stretched, annealed, and poled (OSAP) samples. The QSA films were unidirectionally polarized under 100 MV/m (i.e., 50 MV/m DC + 50 MV/m AC at 1 Hz) for 60 cycles at room temperature. The final thicknesses of all films were 15-30 μm.

#### Structural and Dielectric Characterization

Differential scanning calorimetry (DSC) experiments were carried out on a TA DSC250 (TA Instruments, New Castle, DE). Approximately 2 mg samples were used at a scanning rate of 10 °C/min under a dry nitrogen atmosphere (flow rate of 50 mL/min). For TMDSC, the protocol with a heating rate of 2 °C/min and a modulation amplitude of 0.32 °C for every 60 s was chosen. This protocol has been reported to show high sensitivity and resolution,<sup>26</sup> and thus is suitable for studying microstructure evolution in semicrystalline polymers. Young's modulus along the transverse direction (Y<sub>1</sub>) was determined by stress-strain tests using a Linkam TST350 tensile stage (Linkam Scientific, Surrey, UK) with temperature control. The stretching speed was 25 μm/s. Error bars were obtained as standard deviations from at least three measurements using different samples.

2D SAXS and WAXD experiments were performed at the 11-BM Complex Material Scattering Beamline of the National Synchrotron Light Source II (NSLS-II), Brookhaven National Laboratory (BNL). The wavelength ( $\lambda$ ) of the incident X-ray was 0.0729 nm. The distances between the sample and the WAXD (Pilatus 800 K, Dectris, Gaden-Dattwil, Switzerland) and the SAXS detectors (Pilatus 2M) were 261 and 5050 mm, respectively. These distances were calibrated using silver behenate with the first-order reflection at a scattering vector of  $q = (4\pi \sin\theta)/\lambda = 1.076 \text{ nm}^{-1}$  ( $\theta$  is the half scattering angle). The typical data acquisition time was 30 s. A self-built hot stage was used in temperature-dependent X-ray experiments.

BDS measurement was carried out using a Novocontrol Concept 80 broadband dielectric spectrometer (Novocontrol Technologies, Montabaur, Germany) with temperature control. The applied voltage was  $1.0~V_{rms}$  (i.e., root-mean-square voltage) with frequency ranging from 1 Hz to 1 MHz and temperature from -50 to 100 °C. Gold (Au) electrodes with an area of 7.06 mm<sup>2</sup> were

evaporated on both surfaces of samples using a Quorum Q300T D Plus sputter coater (Quorum Technologies, Ltd., Laughton, East Sussex, UK). The Au electrode thickness was 10 nm.

Simultaneous D-E and S<sub>1</sub>-E loop measurements were conducted using a Premiere II ferroelectric tester (Radiant Technologies, Inc., Albuquerque, NM) with a Trek 10/10B-HS highvoltage amplifier (0-10 kV AC, Trek, Inc., Lockport, NY), as described in a recent report.<sup>27</sup> The applied voltage had a bipolar sinusoidal waveform at 1 Hz. The film samples were coated with gold (Au) electrodes on both sides with an overlapping area of 8×3 mm<sup>2</sup>. The Au-coated film was immersed in silicone oil to avoid corona discharge in air. The stray capacitance was determined using a biaxially oriented polypropylene film (8 µm, provided by SB Electronics, Inc., Barre, VT) with a dielectric constant of 2.25. The final electric displacement was obtained by subtraction of the stray capacitance and AC conduction from the raw data (see Figure S2). The transverse strain, S<sub>1</sub>, of the film samples (initial length of 8 mm) was measured using a home-built fixture connected to a photonic sensor MTI 2100 (MTI Instruments, Inc., Albany, NY), following literature reports.<sup>27,28</sup> At high temperatures (>45 °C), significant conduction was observed in D-E loops due to certain defects (e.g., pinholes) in the large area P(VDF-TrFE) films. To avoid this, separate D-E loop measurements were performed on small-area samples (7.06 mm<sup>2</sup>). A home-built sample fixture was used to connect the Au electrodes on both sides of the film with the interface of the Radiant ferroelectric tester using high-voltage cables. The temperature was controlled using a ChemGlass CG-1999-V-10 hot plate (ChemGlass Life Sciences, LLC, Vineland, NJ). Error bars were obtained as standard deviations from at least three measurements using different samples.

Direct d<sub>33</sub> measurements were carried out using a self-built experimental setup shielded by a Faraday cage, and details should refer our recent report.<sup>8</sup> During the measurement, triboelectricity should be strictly avoided. The generated charge (Q) was measured using a Keithley 617 electrometer (Beaverton, OR, USA). The applied force (F) was measured using a

quartz force sensor (model 208C01, PCB Piezotronics, Depew, NY, USA). Both signals were recorded using a USB data acquisition card (NI USB-6002, National Instruments, USA). The  $d_{33}$  value was determined using equation:  $d_{33} = Q/F$ , when the area of the applied force was the same as the gold electrode area.<sup>8</sup>

#### **ACKNOWLEDGMENTS**

Z.Z. and G.R. contributed equally to this work. L.Z. acknowledges partial financial support for the SAXS and WAXD measurements from National Science Foundation, Division of Materials Research, Polymers Program (DMR-2103196). H.H. acknowledges partial support by the National Natural Science Foundation of China (51873075). E.A. acknowledges the support by the Deutsche Forschungsgemeinschaft (DFG) through Grant AL 2058/1-1. This research used the 11-BM CMS beamline of National Synchrotron Light Source-II (NSLS-II), Brookhaven National Laboratory (BNL), a U.S. Department of Energy User Facility operated for the Office of Science by BNL under Contract DE-SC0012704. The authors thank Dr. Masafumi Fukuto at NSLS-II of BNL for helping SAXS and WAXD experiments

#### **AUTHOR CONTRIBUTIONS**

L.Z., P.L.T., and H.H. conceived the idea and supervised the project. L.Z., Z.Z., and G.R. designed the experiments and wrote the paper. Z.Z. conducted the SAXS, WAXD, D-E/S<sub>1</sub>-E loop, modulus and BDS measurements. Q.L. conducted the DSC measurement. E.A. and P.L.T. performed the computer simulation. R.L. helped the SAXS and WAXD measurements and performed data treatment.

#### DECLARATION OF INTERESTS

The authors declare no competing interests.

## REFERENCES

- 1. Zhang, Q., Huang, C., Xia, F., and Su J. (2004). Electroactive Polymer (EAP) Actuators as Artificial Muscles: Reality, Potential, and Challenges (SPIE Press).
- 2. Li, F., Jin, L., Xu, Z., and Zhang, S. (2014). Electrostrictive effect in ferroelectrics: an alternative approach to improve piezoelectricity. Appl. Phys. Rev. 1, 11103. 10.1063/1.4861260.
- 3. Furukawa, T., and Seo, N. (1990). Electrostriction as the origin of piezoelectricity in ferroelectric polymers. Jpn. J. Appl. Phys. 29, 675-680. 10.1143/JJAP.29.675.
- Katsouras, I., Asadi, K., Li, M., van Driel, T. B., Kjær, K. S., Zhao, D., Lenz, T., Gu, Y., Blom,
   P. W. M., Damjanovic, D. et al. (2016). The negative piezoelectric effect of the ferroelectric polymer poly(vinylidene fluoride). Nat. Mater. 15, 78-84. 10.1038/nmat4423.
- 5. Broadhurst, M. G., and Davis, G. T. (1984). Physical basis for piezoelectricity in PVDF. Ferroelectrics 60, 3-13. 10.1080/00150198408017504.
- 6. Randall, C. A., Kim, N., Kucera, J. P., Cao, W., and Shrout, T. R. (1998). Intrinsic and extrinsic size effects in fine-grained morphotropic-phase-boundary lead zirconate titanate ceramics. J. Am. Ceram. Soc. *81*, 677-688. 10.1111/j.1151-2916.1998.tb02389.x.
- 7. Liu, Y., Aziguli, H., Zhang, B., Xu, W., Lu, W., Bernholc, J., and Wang, Q. (2018). Ferroelectric polymers exhibiting behaviour reminiscent of a morphotropic phase boundary. Nature, *562*, 96-100. 10.1038/s41586-018-0550-z.
- 8. Huang, Y., Rui, G., Li, Q., Allahyarov, E., Li, R., Fukuto, M., Zhong, G., Xu, J., Li, Z., Taylor, P. L. et al. (2021). Enhanced piezoelectricity from highly polarizable oriented amorphous

- fractions in biaxially oriented poly(vinylidene fluoride) with pure  $\beta$  crystals. Nat. Commun. 12, 675. 10.1038/s41467-020-20662-7.
- 9. Fu, Y., Busing, W. R., Jin, Y., Affholter, K. A., and Wunderlich, B. (1994). Structure analysis of the noncrystalline material in poly(ethylene terephthalate) fibers. Macromol. Chem. Phys. *195*, 803-822. 10.1002/macp.1994.021950236.
- Hafner, J., Benaglia, S., Richheimer, F., Teuschel, M., Maier, F. J., Werner, A., Wood, S.,
   Platz, D., Schneider, M., Hradil, K. et al. (2021). Multi-scale characterisation of a ferroelectric polymer reveals the emergence of a morphological phase transition driven by temperature. Nat. Commun. 12, 152. 10.1038/s41467-020-20407-6.
- 11. Tashiro, K., Kobayashi, M., Tadokoro, H., and Fukada, E. (1980). Calculation of elastic and piezoelectric constants of polymer crystals by a point charge model: application to poly(vinylidene fluoride) form I. Macromolecules *13*, 691-698. 10.1021/ma60075a040.
- 12. Barique, M. A., and Ohigashi, H. (2001). Annealing effects on the curie transition temperature and melting temperature of poly(vinylidene fluoride/trifluoroethylene) single crystalline films. Polymer 42, 4981-4987. 10.1016/S0032-3861(00)00937-X.
- 13. Womes, M., Bihler, E., and Eisenmenger, W. (1989). Dynamics of polarization growth and reversal in PVDF films. IEEE Trans. Electr. Insul. *24*, 461-468. 10.1109/14.30890.
- Liu, Y., and Wang, Q. (2020). Ferroelectric polymers exhibiting negative longitudinal piezoelectric coefficient: progress and prospects. Adv. Sci. 7, 1902468.
   10.1002/advs.201902468.
- Gomes, J., Nunes, J.S., Sencadas, V., and Lanceros-Mendez, S. (2010). Influence of the betaphase content and degree of crystallinity on the piezo- and ferroelectric properties of poly(vinylidene fluoride). Smart Mater. Struct. 19, 065010. 10.1088/0964-1726/19/6/065010.

- Oliveira, F., Leterrier, Y., Manson, J.A., Sereda, O., Neels, A., Dommann, A., and Damjanovic, D. (2014). Process influences on the structure, piezoelectric, and gas-barrier properties of PVDF-TrFE copolymer. J. Polym. Sci., Part B: Polym. Phys. 52, 496-506. 10.1002/polb.23443.
- 17. Kepler, R.G., and Anderson, R.A. (1978). Piezoelectricity and pyroelectricity in polyvinylidene fluoride. J. Appl. Phys. 49, 4490-4494. 10.1063/1.325454.
- 18. Furukawa, T. (1989). Piezoelectricity and pyroelectricity in polymers. IEEE Trans. Electr. Insul. 24, 375-394. 10.1109/14.30878.
- 19. Nagai, M., Nakamura, K., Uehara, H., Kanamoto, T., Takahashi, Y., and Furukawa, T. (1999). Enhanced electrical properties of highly oriented poly(vinylidene fluoride) films prepared by solid-state coextrusion. J. Polym. Sci., Part B: Polym. Phys. *37*, 2549-2556. 10.1002/(Sici)1099-0488(19990915)37:18<2549::Aid-Polb1>3.0.Co;2-S.
- Furukawa, T., Wen, J.X., Suzuki, K., Takashina, Y., and Date, M. (1984). Piezoelectricity and pyroelectricity in vinylidene fluoride trifluoroethylene copolymers. J. Appl. Phys. 56, 829-834. 10.1063/1.334016.
- 21. Furukawa, T., and Wen, J.X. (1984). Electrostriction and piezoelectricity in ferroelectric polymers. Jpn. J. Appl. Phys. 23, L677-L679. 10.1143/Jjap.23.L677.
- Wongwirat, T., Zhu, Z., Rui, G., Li, R., Laoratanakul, P., He, H., Manuspiya, H., and Zhu, L. (2020). Origins of electrostriction in poly(vinylidene fluoride)-based ferroelectric polymers.
   Macromolecules 53, 10942-10954. 10.1021/acs.macromol.0c02083.
- 23. Eury, S., Yimnirun, R., Sundar, V., Moses, P. J., Jang, S., and Newnham, R. E. (1999). Converse electrostriction in polymers and composites. Mater. Chem. Phys. *61*, 18-23. 10.1016/S0254-0584(99)00107-8.

- 24. Rui, G., Huang, Y., Chen, X., Li, R., Wang, D., Miyoshi, T., and Zhu, L. (2021). Giant spontaneous polarization for enhanced ferroelectric properties of biaxially oriented poly(vinylidene fluoride) by mobile oriented amorphous fractions. J. Mater. Chem. C *9*, 894-907. 10.1039/D0TC04632A.
- 25. Huang, Y., Xu, J., Soulestin, T., Dos Santos, F. D., Li, R., Fukuto, M., Lei, J., Zhong, G., Li, Z., Li, Y. et al. (2018). Can relaxor ferroelectric behavior be realized for poly(vinylidene fluoride-co-chlorotrifluoroethylene) [P(VDF-CTFE)] random copolymers by inclusion of CTFE units in PVDF crystals? Macromolecules 51, 5460-5472. 10.1021/acs.macromol.8b01155.
- 26. Thomas, L.C. (2005). Modulated DSC paper #6: measurement of initial crystallinity in semicrystalline polymers. (TA Instruments).
- Wongwirat, T., Wang, M., Huang, Y., Treufeld, I., Li, R., Laoratanakul, P., Manuspiya, H., and Zhu, L. (2019). Mesophase structure-enabled electrostrictive property in nylon-12-based poly(ether-block-amide) copolymers. Macromol. Mater. Eng. 304, 1900330. 10.1002/mame.201900330.
- Cheng, Z., Bharti, V., Xu, T., Wang, S., Zhang, Q., Ramotowski, T., Tito, F., and Ting, R. (1999). Transverse strain responses in electrostrictive poly(vinylidene fluoride-trifluoroethylene) films and development of a dilatometer for the measurement. J. Appl. Phys. 86, 2208-2214. 10.1063/1.371032.